# Correlation hole of the spin-polarized electron gas, with exact small-wave-vector and high-density scaling

Yue Wang* and John P. Perdew
*Department of Physics and Quantum Theory Group, Tulane University, New Orleans, Louisiana 70118*
(Received 10 June 1991)

For a uniform electron gas of density $n=n_\uparrow+n_\downarrow=3/4\pi r_s^3=\pi k_s^6/192$ and spin polarization $\zeta=(n_\uparrow-n_\downarrow)/n$, we study the Fourier transform $\bar{\rho}_c(k,r_s,\zeta)$ of the correlation hole, as well as the correlation energy $\varepsilon_c(r_s,\zeta)=\int_0^\infty dk\,\bar{\rho}_c/\pi$. In the high-density ($r_s\to 0$) limit, we find a simple scaling relation $k_s\bar{\rho}_c/\pi g^2\to f(z,\zeta)$, where $z=k/gk_s$, $g=[(1+\zeta)^{2/3}+(1-\zeta)^{2/3}]/2$, and $f(z,1)=f(z,0)$. The function $f(z,\zeta)$ is only weakly $\zeta$ dependent, and its small-$z$ expansion $-3z/\pi^2+4\sqrt{3}z^2/\pi^2+\cdots$ is also the exact small-wave-vector ($k\to 0$) expansion for *any* $r_s$ or $\zeta$. Motivated by these considerations, and by a discussion of the large-wave-vector and low-density limits, we present two Padé representations for $\bar{\rho}_c$ at any $k$, $r_s$, or $\zeta$, one within and one beyond the random-phase approximation (RPA). We also show that $\bar{\rho}_c^{\rm RPA}$ obeys a generalization of Misawa's spin-scaling relation for $\varepsilon_c^{\rm RPA}$, and that the low-density ($r_s\to\infty$) limit of $\varepsilon_c^{\rm RPA}$ is $\sim r_s^{-3/4}$.

## I. INTRODUCTION

The correlation hole surrounding an electron is essentially the real-space analysis of the correlation energy,[1] and its Fourier transform is the corresponding wave-vector analysis[2] (as reviewed in Sec. II). The correlation hole of the uniform electron gas, a quantity of interest in its own right, is also a common ingredient of models for the hole in an inhomogeneous system, e.g., the weighted density approximation[3] or the real-space cutoff of the gradient expansion.[4–6] These models generate useful nonlocal density functionals for the correlation energy[4–6] and potential.[4–7] The aim of the present work is to develop an accurate analytic representation of the Fourier transform for the correlation hole of an electron gas with uniform spin densities $n_\uparrow$ and $n_\downarrow$. In the course of this work, we derive several exact limits and scaling relations for the hole.

The simplest construction which makes sense is the random-phase approximation[8] (RPA), in which the Fourier transform of the hole is defined by an explicit frequency integral (Sec. II) which must be evaluated numerically. We have fitted the result to a Padé approximant (Sec. VII) which reproduces all features except the energetically unimportant second-derivative discontinuity that occurs when the wave vector equals the diameter of the Fermi sphere ($k=2k_F$ for $\zeta=0$). (This unreproduced feature generates long-range oscillations of wave vector $2k_F$ in real space.)

In comparison with accurate values from quantum Monte Carlo calculations,[9] the RPA gives inaccurate correlation energies and unphysical correlation holes[10] at metallic or low electron densities. To go beyond the RPA, we follow the general approach of Nozières and Pines,[11] who used the RPA only in the small-wave-vector or high-density limits (Sec. III) in which it is exact. We modify our Padé representation (Sec. VII) so that it has the correct large-wave-vector (Sec. IV) and low-density (Sec. VI) limiting behaviors, and fits the Monte Carlo correlation energies.[6,9] As a check on our results beyond the RPA, we compare with the Fourier transform of the correlation hole computed from Jastrow-Slater wave functions.[12]

We are not aware of other analytic representations for the correlation hole in wave-vector space. In real space, Contini, Mazzone, and Sacchetti[13] presented an analytic model for the pair-correlation function at full interaction strength $\lambda=1$. However, the correlation hole we seek is the average[1,2] over the range $0\le\lambda\le 1$, where the coupling constant $\lambda$ is the square of the electronic charge. Chacón and Tarazona[14] presented an analytic model of the exchange-correlation hole in real space for a spin-unpolarized uniform electron gas. When the exact exchange hole is subtracted, their model is accurate in the long-range (small-wave-vector) limit and in the domain of metallic densities, but not in the high-density limit. Spin polarization and an accurate account of *both* limits are needed for the construction of a simple generalized gradient approximation for the correlation energy from the real-space cutoff of the gradient expansion for hole. In fact, it is only the occurrence of scaling relations (Sec. III) in these limits which permits[4] the development of an accurate analytic fit to the numerical results of the real-space cutoff.[5,6]

## II. BACKGROUND

Consider a many-electron ground state with inhomogeneous spin densities $n_\uparrow(\mathbf{r})$, $n_\downarrow(\mathbf{r})$. The total density at position $\mathbf{r}$ is

$$n=n_\uparrow+n_\downarrow\ , \tag{1}$$

and the relative spin polarization is

$$\zeta=(n_\uparrow-n_\downarrow)/n\ . \tag{2}$$

The total correlation energy is[1,2]

 

$$E_c=\tfrac{1}{2}\int d^3r\int d^3r'\frac{n(\mathbf{r})n_c(\mathbf{r},\mathbf{r}')}{|\mathbf{r}-\mathbf{r}'|}\ , \tag{3}$$

where $n_c(\mathbf{r},\mathbf{r}')$ is the density at $\mathbf{r}'$ of the correlation hole[1,2] surrounding an electron at $\mathbf{r}$, which obeys the sum rule

$$\int d^3r' n_c(\mathbf{r},\mathbf{r}')=0\ . \tag{4}$$

Only the average hole

$$\bar{n}_c(R)=\frac{1}{N}\int d^3r\, n(\mathbf{r})\int\frac{d\hat{\mathbf{R}}}{4\pi}n_c(\mathbf{r},\mathbf{r}+\mathbf{R}) \tag{5}$$

is needed to evaluate the correlation energy per electron

$$\frac{E_c}{N}=\tfrac{1}{2}\int_0^\infty dR\ 4\pi R^2\frac{\bar{n}_c(R)}{R}\ . \tag{6}$$

In Eq. (5), $N=\int d^3r\, n(\mathbf{r})$ is the number of electrons, and $d\hat{\mathbf{R}}$ denotes the angular element in $\mathbf{R}$ space.

The Fourier or wave-vector analysis of the average hole is

$$\bar{n}_c(R)=\frac{1}{(2\pi)^3}\int_0^\infty dk\ 4\pi k^2\bar{\rho}_c(k)\frac{\sin(kR)}{kR}\ , \tag{7}$$

where the average structure factor

$$\bar{\rho}_c(k)=\int_0^\infty dR\ 4\pi R^2\bar{n}_c(R)\frac{\sin(kR)}{kR} \tag{8}$$

is the Fourier transform of the average correlation hole. When $\bar{n}_c(R)$ is sufficiently localized around $R=0$, Eq.(4) implies that

$$\lim_{k\to 0}\bar{\rho}_c(k)=0\ . \tag{9}$$

Substitution of Eq. (7) into Eq. (6) yields

$$\frac{E_c}{N}=\frac{1}{\pi}\int_0^\infty dk\,\bar{\rho}_c(k)\ . \tag{10}$$

The real-space analysis (6) decomposes the correlation energy into contributions from dynamic density fluctuations at different distances $R$ from an electron, while the wave-vector analysis (10) displays the contributions from fluctuations of different wave vectors $k$.

In a uniform electron gas, the relative spin polarization $\zeta$ and density

$$n=3/4\pi r_s^3=k_F^3/3\pi^2 \tag{11}$$

are independent of $\mathbf{r}$, and

$$E_c/N=\varepsilon_c(r_s,\zeta)\ . \tag{12}$$

The wave-vector analysis within the RPA is easily found from the work of von Barth and Hedin:[8]

$$\bar{\rho}_c^{\,\mathrm{RPA}}(k,r_s,\zeta)=\frac{-6Q^2}{cr_s}\int_0^\infty dW\{\alpha_\zeta(r_s,Q,W)-\ln[1+\alpha_\zeta(r_s,Q,W)]\}\ , \tag{13}$$

where

$$Q=k/2k_F \tag{14a}$$

and

$$W=\omega/2k_F^2 \tag{14b}$$

are the reduced wave vector and frequency, respectively. Here $c=(4/9\pi)^{1/3}$, and $k_F=1/cr_s$ is the Fermi wave vector. Also

$$\alpha_\zeta(r_s,Q,W)=\frac{cr_s}{4\pi}[x_1\beta(x_1Q,x_1^2W)+x_2\beta(x_2Q,x_2^2W)]\ , \tag{15}$$

where

$$x_1=(1+\zeta)^{-1/3}\ , \tag{16}$$

$$x_2=(1-\zeta)^{-1/3}\ , \tag{17}$$

$$\beta(Q,W)=\frac{1}{Q^2}\left\{1+\frac{W^2+Q^2-Q^4}{4Q^3}\ln\left[\frac{W^2+Q^2(1+Q)^2}{W^2+Q^2(1-Q)^2}\right]-\frac{W}{Q}\left[\tan^{-1}\left[\frac{Q^2+Q}{W}\right]-\tan^{-1}\left[\frac{Q^2-Q}{W}\right]\right]\right\}\ . \tag{18}$$

For later use, we define the Thomas-Fermi screening wave vector

$$k_s=(4k_F/\pi)^{1/2}\ , \tag{19}$$

and display the Fourier transform of the *exchange* hole:

$$\bar{\rho}_x(k,r_s,\zeta)=\tfrac{1}{2}(1+\zeta)F_x((1+\zeta)^{-1/3}Q)+\tfrac{1}{2}(1-\zeta)F_x((1-\zeta)^{-1/3}Q)\ , \tag{20}$$

where

$$F_x(Q)=\begin{cases}-1+3Q/2-Q^3/2, & 0\le Q\le 1\\ 0, & Q>1\ .\end{cases} \tag{21}$$

The small-wave-vector expansion of Eq. (20) is

$$\bar{\rho}_x(k,r_s,\zeta)\to -1+3gQ/2-Q^3/2\ , \tag{22}$$

where

$$g(\zeta)=[(1+\zeta)^{2/3}+(1-\zeta)^{2/3}]/2\ . \tag{23}$$

Note that the second-derivative discontinuity of Eq. (21) at $Q=1$ is not included in the Padé representation

$$F_x(Q)=\frac{-1}{1+1.5Q+2.25Q^2+2.875Q^3+3.5625Q^4+24.88Q^5}\ , \tag{24}$$

which reproduces the first four derivatives of $F_x$ at $Q=0$ plus the integral of $F_x(Q)$ from 0 to $\infty$.

All our equations are expressed in atomic units. The unit of distance is 1 bohr$=a_0=\hbar^2/me^2$, and the unit of energy is 1 hartree$=e^2/a_0$, where $e$ and $m$ are the charge and mass of the electron. With this understanding, our equations apply for any values of $e^2$ and $m$, not just the physical ones. For example, the high-density limit of Sec.

III means $na_0^3 \to \infty$, and may be achieved by $n \to \infty$, $e^2 \to 0$, or $m \to 0$.

## III. SMALL-WAVE-VECTOR AND HIGH-DENSITY SCALING

We seek the $k \to 0$ or $k_F \to \infty$ behavior of the RPA equations (13)–(19). In either limit, $Q \to 0$. Following Gell-Mann and Brueckner,[15] we find for $Q \ll 1$

$$\beta(Q,W)=\frac{2}{Q^2}R(u)+\begin{cases}O(Q^0u^0), & u<1\\ O(Q^0u^{-2}), & u>1\end{cases}, \tag{25}$$

where

$$u=W/Q\ , \tag{26}$$

$$R(u)=1-u\tan^{-1}(u^{-1})\ . \tag{27}$$

From Eq. (25),

$$\int_0^\infty dW\,\alpha_\xi(r_s,Q,W)=\frac{cr_s}{8Q}(x_1^{-2}+x_2^{-2})+O(Q)\ , \tag{28}$$

and thus

$$\rho_c^{\mathrm{RPA}}(k,r_s,\xi)=-\tfrac{3}{2}g(\xi)Q+O(Q^3)+\frac{6Q^3}{cr_s}\int_0^\infty du\,\ln\left[1+\frac{cr_s}{2\pi Q^2}\left[\frac{1}{x_1}R(x_1u)+\frac{1}{x_2}R(x_2u)\right]\right]\ . \tag{29}$$

To evaluate the integral in Eq. (29), we assume $x_1 \geq x_2$ without loss of generality. As $u$ varies from 0 to $\infty$, the function $R(u)$ decreases monotonically from 1 to 0. Thus for $u \leq 1/x_2$, the integrand will be dominated by

$$\ln\left[1+\frac{cr_s}{2\pi Q^2}\left[\frac{1}{x_1}R(x_1u)+\frac{1}{x_2}R(x_2u)\right]\right]\approx\ln\left[\frac{cr_s}{2\pi Q^2}\left[\frac{1}{x_1}R(x_1u)+\frac{1}{x_2}R(x_2u)\right]\right]+O(Q^2)\ . \tag{30}$$

For $u > 1/x_2$, we expand the functions $R(x_1u)$ and $R(x_2u)$ to all orders in $(x_1u)^{-1}$ and $(x_2u)^{-1}$, respectively. After some tedious analysis, we find

$$\bar{\rho}_c^{\mathrm{RPA}}(k,r_s,\xi)=-\tfrac{3}{2}g(\xi)Q+2\left[\frac{3\pi}{cr_s}\right]^{1/2}Q^2+O(Q^3)\ . \tag{31}$$

The term of Eq. (31) linear in $Q$ is well known, at least[16,17] for the spin-unpolarized case $\xi=0$: it cancels a similar term in the Fourier transform of the exchange hole [Eq. (22)]. Similarly, the long-range ($R \to \infty$) nonoscillatory behavior ($\sim R^{-4}$) of the correlation hole cancels that of the exchange hole, as a result of screening. The $Q^2$ term in Eq. (31) is also known[16,17] in the special case $\xi=0$. Since this $Q^2$ term arises from plasmon zero-point energy,[16,17] it is independent of $\xi$.

Note the appearance of $\sqrt{r_s}$ in Eq. (31). There are two wave-vector scales: the Fermi wave vector $k_F$, and the screening wave vector $k_s$ of Eq. (19). It is convenient to rewrite Eq. (31) as

$$\frac{k_s\bar{\rho}_c(k,r_s,\xi)}{\pi g^2}=\frac{-3}{\pi^2}z+\frac{4\sqrt{3}}{\pi^2}z^2+O(z^3)\ , \tag{32}$$

where

$$z=k/gk_s\ . \tag{33}$$

The leading terms of Eq. (32) depend on $z$, but not otherwise on $r_s$ or $\xi$.

In this high-density limit $r_s \to 0$, where $k_F$ diverges faster than $k_s$, we expect that the only important wave-vector scale will be $k_s$, and Eq. (32) will sum to

$$k_s\bar{\rho}_c(k,r_s,\xi)/\pi g^2 \to f(z,\xi)\ . \tag{34}$$

Moreover, we will show in Sec. V that

$$f(z,1)=f(z,0)\ . \tag{35}$$

Our numerical study of the RPA (Table I) confirms Eqs. (34) and (35), and further indicates that the $\xi$ dependence of $f$ is very weak: In the high-density limit,

$$k_s\bar{\rho}_c(k,r_s,\xi)/\pi g^2 \approx f(z,0)\ . \tag{36}$$

The corresponding high-density limit of the correlation hole is

$$\bar{n}_c^{\mathrm{RPA}}(R)\approx g^3(gk_s)^2A_c^{\mathrm{RPA}}(gk_sR)\ . \tag{37}$$

The right-hand side of Eq. (37) is also the exact form for the long-range nonoscillatory behavior of the correlation hole [since this behavior is controlled by the small-wave-vector behavior of $\bar{\rho}_c$, Eq. (32)]. Following the general ideas of Refs. 11 and 15, we expect the new scaling relations (32)–(36) to remain valid beyond the RPA.

By substituting Eq. (36) into Eq. (10), we find that the high-density limit of the correlation energy scales approximately like $g^3$. The exact analytic behavior in the high-density limit is[18]

$$\varepsilon_c(r_s,\xi)=0.031\,09I(\xi)\ln r_s+O(r_s^0)\ , \tag{38}$$

where

$$I(\xi)=\frac{1}{2}\left[1+\frac{x_1^{-1}x_2^{-1}(x_1^{-1}+x_2^{-1})-(1+\xi)\ln x_1-(1-\xi)\ln x_2-2\ln(x_1^{-1}+x_2^{-1})}{2(1-\ln 2)}\right]\ . \tag{39}$$

TABLE I. Comparison of the Padé approximation [Eq. (42)] with the exact [Eq. (13)] $-1000k_s\bar{\rho}_c^{\mathrm{RPA}}(k,r_s,\zeta)/\pi g(\zeta)^2$ near the high-density limit ($r_s=10^{-7}$), in a.u., for various values of $\zeta$ and $z=k/gk_s$.

| | | $z$ | | | | | | |
|---|---|---|---|---|---|---|---|---|
| $\zeta$ | Method | 0.1 | 0.6 | 1.0 | 2.0 | 4.0 | 6.0 | 10.0 |
| 0.0 | Exact | 24.14 | 51.53 | 44.43 | 28.04 | 15.09 | 10.21 | 6.17 |
| | Padé | 24.14 | 51.21 | 44.27 | 27.94 | 14.94 | 10.09 | 6.11 |
| 0.3 | Exact | 24.14 | 51.64 | 44.58 | 28.18 | 15.17 | 10.26 | 6.21 |
| | Padé | 24.15 | 51.26 | 44.34 | 28.02 | 15.00 | 10.14 | 6.14 |
| 0.6 | Exact | 24.15 | 51.97 | 45.04 | 28.58 | 15.42 | 10.43 | 6.31 |
| | Padé | 24.15 | 51.41 | 44.57 | 28.27 | 15.18 | 10.27 | 6.23 |
| 0.9 | Exact | 24.16 | 52.31 | 45.57 | 29.09 | 15.73 | 10.65 | 6.44 |
| | Padé | 24.15 | 51.60 | 44.86 | 28.59 | 15.41 | 10.45 | 6.34 |
| 1.0 | Exact | 24.14 | 51.55 | 44.45 | 28.06 | 15.10 | 10.22 | 6.18 |
| | Padé | 24.14 | 51.21 | 44.27 | 27.94 | 14.94 | 10.09 | 6.11 |

To order $\ln r_s$, the RPA correlation energy is exact.[15] As shown in Ref. 18, the functions $I$ and $g^3$ are equal for $\zeta=0$ and 1, and roughly equal for intermediate values of $\zeta$. Except at $\zeta=0$ and 1, the function $g(\zeta)$ [Eq. (23)], which enters the scaling relations (32–(36), differs from the more obvious candidate

$$\tilde{g}(\zeta)=\{[(1+\zeta)^{1/3}+(1-\zeta)^{1/3}]/2\}^{1/2}\ , \tag{40}$$

which enters the static Thomas-Fermi dielectric function:

$$\varepsilon_{\mathrm{TF}}(k)=1+(\tilde{g}k_s/k)^2\ . \tag{41}$$

In fact, $\tilde{g}^3\geq I\geq g^3$, and $I\approx(\tilde{g}^3 g^3)^{1/2}$.

We can accurately represent the high-density limit $f(z,\zeta)$ of Eq. (34) by a Padé approximant:

$$f(z,\zeta)=\frac{\alpha_1 z+\alpha_2 z^2+\alpha_3 z^3}{\left[1+\beta_1 z+\beta_2\left[\frac{g^3}{I}\right]^{1/2}z^2\right]^2}\ . \tag{42}$$

From the small-wave-vector limit of Eq. (32),

$$\alpha_1=-\frac{3}{\pi^2}=-0.303\,964\ , \tag{43}$$

$$\alpha_2-2\alpha_1\beta_1=4\sqrt{3}/\pi^2\ . \tag{44}$$

The correlation energy in the high-density limit is essentially

$$\varepsilon_c(r_s,\zeta)\to g^3\int_0^{z_c(r_s)}dz\,f(z,\zeta)\ , \tag{45}$$

where the cutoff $z_c(r_s)\sim r_s^{-1/2}$ occurs as $k$ approaches $2k_F$. The $z^{-1}$ asymptote of Eq. (42) yields the $\ln r_s$ term of Eq. (38), provided that

$$-\tfrac{1}{2}\alpha_3/\beta_2^2=0.031\,09\ . \tag{46}$$

Given conditions (43), (44), and (46), there are only two independent parameters in Eq. (42), which are fixed by a least-squares fit to our numerical RPA result at $\zeta=0$ and small $r_s$ (Table I). We find, in addition to Eq. (43),

$$\alpha_2=-0.181\,18\ , \tag{47}$$

$$\alpha_3=-0.076\,53\ , \tag{48}$$

$$\beta_1=1.452\,73\ , \tag{49}$$

$$\beta_2=1.109\,38\ . \tag{50}$$

[Equation (42) is in fact a reduced form in the high-density limit of a general Padé for any density, Eq. (71); an equally good fit to the high-density limit can be found from a simple [2/3] Padé form.]

## IV. LARGE-WAVE-VECTOR BEHAVIOR

Here we will show that, in the limit $k\to\infty$ (and thus $k\gg k_s$, $k\gg k_F$),

$$\bar{\rho}_c^{\mathrm{RPA}}(k,r_s,\zeta)\sim r_s Q^{-4}\ . \tag{51}$$

Qualitatively similar behavior is expected beyond the RPA, where the limit (51) implies a cusp[19] in the correlation hole at $R=0$.

We expand Eq. (18) in powers of $Q^{-1}$ and collect like terms to find

$$\beta(Q,W)=\frac{2}{3}\frac{Q^{-4}}{1+v^2}+\frac{16(v^2-1)}{(1+v)^4}Q^{-5}+O(Q^{-6})\ , \tag{52}$$

where

$$v=W/Q^2\ . \tag{53}$$

Now it follows from Eqs. (13) and (15) that

$$\begin{aligned}\bar{\rho}_c^{\mathrm{RPA}}(k,r_s,\zeta)&=\frac{-3Q^2}{cr_s}\int_0^\infty dW\,\alpha_\zeta(r_s,Q,W)^2+O(Q^{-10})\\&=\frac{-cr_s}{12\pi}Q^{-4}+\frac{15}{8\pi}cr_sQ^{-5}h(\zeta)+O(Q^{-6})\ ,\end{aligned} \tag{54}$$

in agreement with Eq. (51), where

$$h(\zeta)=[(1+\zeta)^{4/3}+(1-\zeta)^{4/3}]/2 \ . \tag{55}$$

Equation (54) is presumably useful when $Q$ is so large that the $Q^{-5}$ term is smaller in magnitude than the $Q^{-4}$ term, i.e., when

$$Q>45h/2\geq 45/2 \ . \tag{56}$$

Since the Fourier transform of the hole is normally negligible for $Q>45/2$, the details of the limit (54) are not very useful for the Padé representation of $\bar{\rho}_c$, and only the general behavior (51) will be imposed.

## V. GENERALIZED MISAWA SCALING IN THE RPA

Misawa[20] has shown that, for all $r_s$,

$$\varepsilon_c^{\mathrm{RPA}}(r_s,1)=\tfrac{1}{2}\varepsilon_c^{\mathrm{RPA}}(2^{-4/3}r_s,0) \ . \tag{57}$$

Here we will derive an analogous relationship satisfied by $\bar{\rho}_c(k,r_s,\zeta)$ within (but not beyond) the RPA.

First note that, as $\zeta\to 1$, $x_2\to\infty$ by Eq. (17). Thus, by Eq. (52),

$$x_2\beta(x_2Q,x_2^{\frac{2}{3}}W)=x_2^{\frac{2}{3}}(x_2Q)^{-4}/(1+v^2)\to 0 \tag{58}$$

for any $v$ and $Q$. Therefore

$$\alpha_1(r_s,Q,W)=\frac{cr_s}{4\pi}2^{-1/3}\beta(2^{-1/3}Q,2^{-2/3}W) \ . \tag{59}$$

It follows from Eq. (13), after change of integration variable from $W$ to $W'=2^{-2/3}W$, that

$$\bar{\rho}_c^{\mathrm{RPA}}(k,r_s,1)=\frac{-6Q^2}{cr_s}\int_0^\infty dW' 2^{2/3}\left[\frac{cr_s}{4\pi}2^{-1/3}\beta(2^{-1/3}Q,W')-\ln\left[1+\frac{cr_s}{4\pi}2^{-1/3}\beta(2^{-1/3}Q,W')\right]\right] \ . \tag{60}$$

Comparison of Eq. (60) with

$$\bar{\rho}_c^{\mathrm{RPA}}(k,r_s,0)=\frac{-6Q^2}{cr_s}\int_0^\infty dW\left[\frac{cr_s}{2\pi}\beta(Q,W)-\ln\left[1+\frac{cr_s}{2\pi}\beta(Q,W)\right]\right] \tag{61}$$

leads to the conclusion

$$\bar{\rho}_c^{\mathrm{RPA}}(k,r_s,1)=\bar{\rho}_c^{\mathrm{RPA}}(2k,2^{-4/3}r_s,0) \ . \tag{62}$$

Integration of Eq. (62) over $k$, combined with Eq. (10), implies the original Misawa relation (57). It is easy to check that Eq. (54) obeys the generalized Misawa relation (62). The high-density limit of Eq. (34) must also obey this relation, which implies Eq. (35).

## VI. LOW-DENSITY LIMIT

As the density $n$ tends to zero, the ratio $k_s/k_F$ diverges. We expect that the only relevant wave-vector scale in this limit is $k_F$, i.e.,

$$\bar{\rho}_c(k,r_s,0)\to F_c(Q) \tag{63}$$

as $r_s\to\infty$, a result consistent with Eq. (31). Then Eq. (10) would seem to imply

$$\varepsilon_c(r_s,0)\to\gamma/r_s \ , \tag{64}$$

where

$$\gamma=\frac{2}{\pi c}\int_0^\infty dQ\, F_c(Q) \ . \tag{65}$$

These expectations are apparently satisfied *beyond* the RPA. In a Monte Carlo study, Ceperley found the low-density limit for the exchange-correlation energy of a uniform electron gas to be[21]

$$\varepsilon_{xc}(r_s,0)=\frac{-0.8851}{r_s}+\frac{1.435}{r_s^{3/2}}+O(r_s^{-2}) \ , \tag{66}$$

$$\varepsilon_{xc}(r_s,1)=\frac{-0.885}{r_s}+\frac{1.420}{r_s^{3/2}}+O(r_s^{-2}) \ . \tag{67}$$

Although intermediate values of $\zeta$ were not examined, it appears that, to order $r_s^{-1}$, $\varepsilon_{\mathrm{xc}}(r_s,\zeta)$ is independent of $\zeta$. That is not an unexpected result, since the exact change-correlation energy in the low-density limit is essentially the electrostatic energy of the Wigner lattice. Subtraction of the exchange energy

$$\varepsilon_x(r_s,\zeta)=\frac{-3}{4\pi cr_s}h(\zeta) \tag{68}$$

from $\varepsilon_{\mathrm{xc}}(r_s,\zeta)=\varepsilon_{\mathrm{xc}}(r_s,0)$ then implies that

$$\varepsilon_c(r_s,\zeta)\to\frac{-0.8851}{r_s}[1-0.5177h(\zeta)] \tag{69}$$

as $r_s\to\infty$.

The standard analytic parametrizations[8,22,23] of the RPA correlation energy assume that Eq. (64) is also valid *within* the RPA. Surprisingly, our numerical and analytic studies show that

$$\varepsilon_c^{\mathrm{RPA}}(r_s,\zeta)\to -0.40/r_s^{3/4} \tag{70}$$

as $r_s\to\infty$. [The $\zeta$ independence of Eq. (70) is consistent with the Misawa scaling relation (57).] This discovery has motivated a more accurate parametrization[6] of $\varepsilon_c^{\mathrm{RPA}}(r_s,\zeta)$.

The reason for the failure of the expectation (64) within the RPA is the divergence of the integral defined in Eq. (65). From our numerical studies for $r_s\leq 10^6$, it appears that $F_c^{\mathrm{RPA}}(Q)=-1-F_x(Q)$, where $F_x(Q)$ is the Fourier transform of the exchange hole. In other words, the

RPA exchange-correlation hole $\bar{n}_{xc}^{RPA}(R)$ tends to a delta function $-\delta(\mathbf{R})$ (on the scale of the Fermi wavelength) in the low-density limit. This is obviously an unphysical feature of the RPA, since the true exchange-correlation hole cannot be more negative than $-n$. Only in the low-density limit ($k_F \ll k_s$) can the RPA "screen out" all of the exchange hole, including all of its second-derivative discontinuity at $k=2k_F$.

In the Appendix, we present an analytic derivation of the $r_s^{-3/4}$ dependence of Eq. (70).

## VII. PADÉ REPRESENTATION FOR ARBITRARY DENSITIES

As a possible generalization of Eqs. (34) and (42) away from the high-density limit, consider

$$\frac{k_s\bar{\rho}_c(k,r_s,\zeta)}{\pi g^2}=\frac{\alpha_1 z+\alpha_2 z^2+\alpha_3 z^3+\alpha_4(\zeta)r_s^{1/2}z^4}{\left[1+\beta_1 z+\beta_2\left[\frac{g^3}{I}\right]^{1/2}z^2+\beta_3(\zeta)r_s^p z^3+\beta_4(\zeta)r_s z^4\right]^2}, \tag{71}$$

where $p>1$, and $\alpha_4(\zeta)$, $\beta_3(\zeta)$, and $\beta_4(\zeta)$ are functions to be determined. Clearly, Eq. (71) reduces to Eq. (42) in the high-density limit $r_s\to 0$, and to Eq. (32) in the small-wave-vector limit $k\to 0$. Moreover, Eq. (71) satisfies the large-wave-vector limit of Eq. (51), i.e., neglecting the $\zeta$ dependence,

$$k_s\bar{\rho}_c(k,r_s,\zeta)/\pi g^2 - r_s^{-3/2}z^{-4} \tag{72}$$

as $k\to\infty$.

To study the low-density limit $r_s\to\infty$, we change variable from $z$ to $Q$. In this limit, Eq. (71) reduces to

$$\bar{\rho}_c(k,r_s,\zeta)\to -\tfrac{3}{2}gQ/(1+BQ^3)^2 , \tag{73}$$

where

$$B=\left[\frac{\pi}{c}\right]^{3/2}\frac{\beta_3}{g^3}r_s^{p-3/2} . \tag{74}$$

The low-density limit of the correlation energy is then

$$\frac{2k_F}{\pi}\int_0^\infty dQ\frac{-\frac{3}{2}gQ}{(1+BQ^3)^2}=\frac{-3g}{\pi c r_s}\frac{(2\sqrt{3}\pi/27)}{B^{2/3}} . \tag{75}$$

Within the RPA, we equate Eqs. (75) and (70) to find

$$p^{RPA}=\tfrac{9}{8} , \tag{76}$$

$$\beta_3^{RPA}(\zeta)=C_0^{RPA}g^{9/2} . \tag{77}$$

where the *a priori* value of $C_0^{RPA}$ is 0.17. Beyond the RPA, we equate Eqs. (75) and (69) to find

$$p=\tfrac{3}{2} , \tag{78}$$

$$\beta_3(\zeta)=C_0 g^{9/2}(1-C_1 h)^{-3/2} , \tag{79}$$

where the *a priori* constants are $C_0=0.0515$ and $C_1=0.5177$.

It remains to determine the functions $\alpha_4(\zeta)$ and $\beta_4(\zeta)$, which we assume are of the form

$$\alpha_4(\zeta)=\sum_{n=0}^{4}a_{2n}\zeta^{2n} , \tag{80}$$

$$\beta_4(\zeta)=\sum_{n=0}^{4}b_{2n}\zeta^{2n} . \tag{81}$$

The coefficients in Eqs. (80) and (81) are chosen by a least-squares fit to the correlation energies $\varepsilon_c(r_s,\zeta)$.

Within the RPA, we fit to the exact numerical $\varepsilon_c^{RPA}(r_s,\zeta)$ at $r_s=0.5$, 1, 2, 5, 10, 20, 50, and 100 for $\zeta=0.0$, 0.2, 0.4, 0.6, 0.8, and 1.0, as tabulated by Vosko, Wilk, and Nusair.[22] [More precisely, we minimize the square absolute error of Eq. (71) separately for each $\zeta$, then minimize the square absolute error of Eqs. (80) and (81)]. We vary not only the coefficients in Eqs. (80) and (81) but also $C_0^{RPA}$ of Eq. (77), and find

$$C_0^{RPA}=0.2055 , \tag{82}$$

$$\alpha_4^{RPA}(\zeta)=-0.001\,79(1+12.332\zeta^2+6.909\zeta^4-9.359\zeta^6-10.252\zeta^8) , \tag{83}$$

$$\beta_4^{RPA}(\zeta)=0.1279(1+0.473\zeta^2+0.0585\zeta^4-0.0929\zeta^6-1.0417\zeta^8) . \tag{84}$$

Because $\alpha_4^{RPA}(1)=2^{-2/3}\alpha_4(0)$ and $\beta_4^{RPA}(1)=2^{-4/3}\beta_4(0)$, the RPA Padé (71) satisfies the generalized Misawa scaling relation of Eq. (62).

Figure 1 compares the RPA Padé approximation (71) against the exact numerical RPA result. The Padé representation is accurate, apart from a "crossover" behavior. This crossover is to be expected, because the Padé form cannot reproduce the second-derivative discontinuity of the exact numerical RPA, which occurs at $k=2k_F$ when $\zeta=0$, and at $k=2^{4/3}k_F$ when $\zeta=1$. Table II compares the RPA correlation energies generated by the Padé (71) and Eq. (10) against the exact numerical RPA correlation energies,[22] and also the analytic representations of $\varepsilon_c^{RPA}(r_s,\zeta)$ by Vosko, Wilk, and Nusair[22] (VWN) and Perdew and Wang[6] (PW). The Padé values for $\varepsilon_c^{RPA}(r_s,\zeta)$ are more accurate than the VWN value, especially for large $r_s$. This reflects the fact that our Padé yields the correct low-density limit of Eq. (70), while the VWN analytic representation does not.

Beyond the RPA, we would like to follow the same fitting procedure, replacing the numerical RPA correlation energies $\varepsilon_c^{RPA}(r_s,\zeta)$ by Monte Carlo values $\varepsilon_c(r_s,\zeta)$. While the latter are known[9] only for $\zeta=0$ and 1, a plausible interpolation in $\zeta$ has been presented by VWN.[22] We

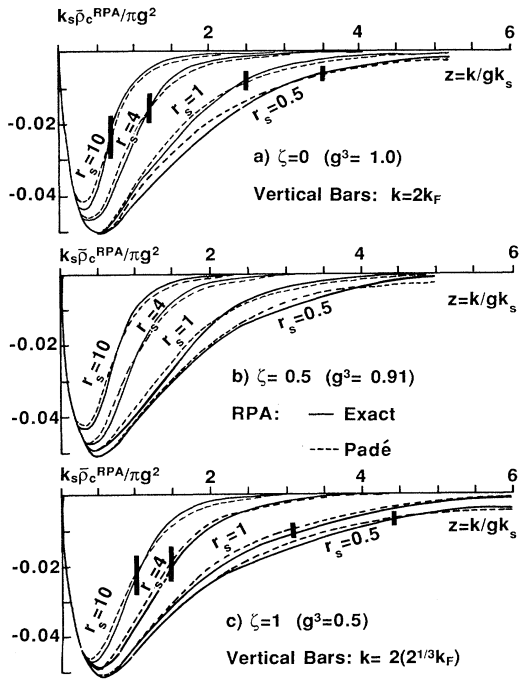


FIG. 1. Scaled Fourier transform $k_s\bar{\rho}_c^{\mathrm{RPA}}(k,r_s,\zeta)/\pi g^2$ of the RPA correlation hole vs scaled wave vector $z=k/gk_s$, from the exact RPA Eq. (13) (solid curves) and from the RPA Padé representation (71) (dashed curves). By Eq. (10), the area under each curve is the spin-scaled correlation energy $\varepsilon_c^{\mathrm{RPA}}(r_s,\zeta)/g^3$, in atomic units.

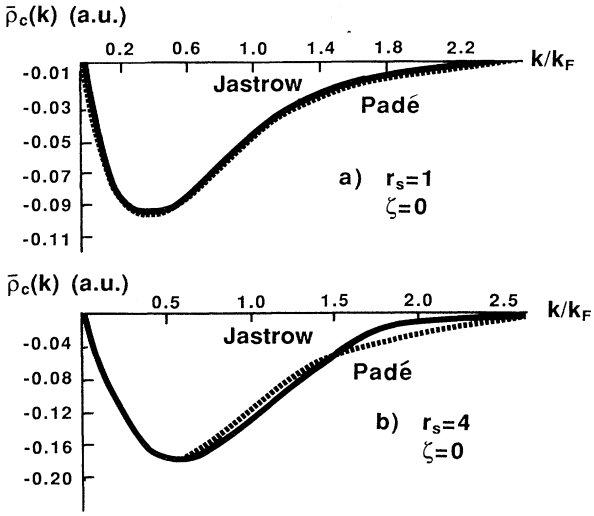


FIG. 2. Fourier transform $\bar{\rho}_c(k,r_s,\zeta)$ of the correlation hole vs reduced wave vector $k/k_F$, from a Jastrow-Slater wavefunction variational calculation, as plotted in Ref. 12 (solid curves), and from the beyond-RPA Padé representation (71) (dashed curves).

have developed our own (PW) analytic representation[6] for $\varepsilon_c(r_s,\zeta)$, which is numerically very close to that of VWN, and we fit to the PW values at $r_s=0.5$, 1, 2, 5, 10, 20, 50, and 100 for $\zeta=0.0$, 0.2, 0.4, 0.6, 0.8, and 1.0. We vary not only the coefficients in Eqs. (80) and (81), but also $C_0$ and $C_1$ of Eq. (79), and find

$$C_0=0.0589\ , \tag{85}$$

TABLE II. $(-1)\times$RPA correlation energy $\varepsilon_c^{\mathrm{RPA}}(r_s,\zeta)$ in mRy. (2000 mRy=1 hartree.) Padé: Eq. (71). Exact: Eq. (13). PW: analytic representations of Ref. 6. VWN: analytic representation of Ref. 22.

| | | ζ | | | | | |
|---|---|---|---|---|---|---|---|
| $r_s$ | Method | 0.0 | 0.2 | 0.4 | 0.6 | 0.8 | 1.0 |
| 0.5 | Padé | 194.6 | 192.8 | 187.2 | 176.7 | 159.8 | 123.6 |
| | Exact | 194.6 | 192.7 | 186.6 | 175.5 | 158.1 | 123.7 |
| | PW | 194.4 | 192.5 | 186.4 | 175.6 | 157.4 | 123.6 |
| | VWN | 195.3 | 193.3 | 187.3 | 176.4 | 158.0 | 123.6 |
| 2 | Padé | 123.6 | 122.5 | 119.2 | 113.0 | 103.3 | 84.8 |
| | Exact | 123.6 | 122.5 | 118.9 | 112.5 | 102.6 | 84.8 |
| | PW | 123.6 | 122.4 | 118.9 | 112.6 | 102.4 | 84.8 |
| | VWN | 124.9 | 123.8 | 120.2 | 113.9 | 103.5 | 85.0 |
| 5 | Padé | 85.0 | 84.3 | 82.2 | 78.4 | 72.4 | 62.0 |
| | Exact | 84.9 | 84.2 | 82.0 | 78.1 | 72.1 | 62.0 |
| | PW | 85.0 | 84.3 | 82.0 | 78.2 | 72.1 | 62.0 |
| | VWN | 86.2 | 85.5 | 83.3 | 79.3 | 73.1 | 62.3 |
| 100 | Padé | 16.5 | 16.5 | 16.3 | 15.9 | 15.3 | 14.5 |
| | Exact | 16.6 | 16.5 | 16.3 | 15.9 | 15.4 | 14.5 |
| | PW | 16.6 | 16.6 | 16.3 | 16.0 | 15.4 | 14.5 |
| | VWN | 15.0 | 15.0 | 14.7 | 14.4 | 14.0 | 13.9 |

TABLE III. $(-1)\times$beyond-RPA correlation energy $\varepsilon_c(r_s,\zeta)$ in mRy. See caption of Table II. PZ: analytic representation of Ref. 14.

| | | $\zeta$ | | | | | |
|---|---|---|---|---|---|---|---|
| $r_s$ | Method | 0.0 | 0.2 | 0.4 | 0.6 | 0.8 | 1.0 |
| 0.5 | Padé | 153.3 | 151.3 | 145.5 | 134.6 | 116.2 | 80.5 |
| | PW | 153.2 | 151.2 | 145.0 | 133.9 | 115.2 | 80.4 |
| | VWN | 154.1 | 152.1 | 145.9 | 134.8 | 115.9 | 80.2 |
| | PZ | 152.1 | 149.7 | 142.2 | 129.3 | 110.0 | 80.6 |
| 2 | Padé | 89.3 | 88.1 | 84.5 | 77.9 | 67.1 | 47.6 |
| | PW | 89.5 | 88.3 | 84.4 | 77.7 | 66.8 | 47.8 |
| | VWN | 89.6 | 88.4 | 84.7 | 78.1 | 67.2 | 47.7 |
| | PZ | 90.2 | 88.7 | 84.4 | 76.8 | 65.4 | 48.2 |
| 5 | Padé | 56.5 | 55.8 | 53.4 | 49.3 | 42.6 | 31.0 |
| | PW | 56.4 | 55.6 | 53.2 | 48.8 | 42.1 | 30.9 |
| | VWN | 56.3 | 55.5 | 53.2 | 49.0 | 42.4 | 30.9 |
| | PZ | 56.7 | 55.8 | 53.1 | 48.5 | 41.6 | 31.0 |
| 100 | Padé | 6.0 | 5.9 | 5.7 | 5.3 | 4.7 | 3.8 |
| | PW | 6.4 | 6.3 | 6.1 | 5.7 | 5.1 | 4.1 |
| | VWN | 6.4 | 6.3 | 6.1 | 5.6 | 5.0 | 4.1 |
| | PZ | 6.3 | 6.3 | 6.0 | 5.6 | 5.0 | 4.1 |

$$C_1=0.5693\ , \tag{86}$$

$$\alpha_4(\zeta)=-0.1057(1+0.7422\zeta^2+0.6510\zeta^4 -0.6406\zeta^6-0.4176\zeta^8)\ , \tag{87}$$

$$\beta_4(\zeta)=0.8796(1+0.3674\zeta^2-0.2557\zeta^4 +1.3072\zeta^6-1.3698\zeta^8)\ . \tag{88}$$

Figure 2 compares the beyond-RPA Padé (71) against the result[12] of a Jastrow-Slater wave-function variational calculation. As in the RPA, there is good agreement apart from a crossover at $k\approx 2k_F$. Table III compares the beyond-RPA correlation energies generated by Eqs. (71) and (10) against those from the PW analytic representation[6] of $\varepsilon_c(r_s,\zeta)$, that of VWN,[22] and that of Perdew and Zunger[24] (PZ).

Figure 3 compares the real-space correlation holes $\bar{n}_c(R)$ within and beyond the RPA for $\zeta=0$ and $r_s=4$. These curves were generated by inverse Fourier transformation [Eq. (7)] of the Padé form (71). As expected,[10] the RPA hole is too deep close to the electron, but correct far away.

In summary, our Padé representation for the Fourier transform of the correlation hole is Eq. (71), supplemented by Eqs. (23), (33), (39), (43), and (47)–(50). Within the RPA, we use Eqs. (76), (77), and (80)–(84). Beyond the RPA, we use Eqs. (55), (78), (79), and (85)–(88). By construction, Eq. (71) obeys the exact scaling relations (32)–(36). (For other scaling relations obeyed by the correlation hole, see Ref. 25.)

Finally, we recall that the correlation hole $\bar{n}_c(R,r_s,\zeta)$ and its Fourier transform $\bar{\rho}_c(k,r_s,\zeta)$ are averages over a coupling constant.[1,2,16] The Fourier transform of the Coulomb hole density, which expresses the real pair correlations of the electron gas at the physical coupling constant, may be constructed by the following prescription:[6] First write

$$\bar{\rho}_c(k,r_s,\zeta)=J(Q,r_s,\zeta)\ , \tag{89}$$

and then construct

$$J(Q,r_s,\zeta)+r_s\frac{\partial}{\partial r_s}J(Q,r_s,\zeta)\ . \tag{90}$$

Starting from Eq. (71), the first step is achieved by the substitutions $k_s\rightarrow 1.563\,185 r_s^{-1/2}$ and $z\rightarrow 2.455\,446 r_s^{-1/2}Q/g$, and the second step generates the

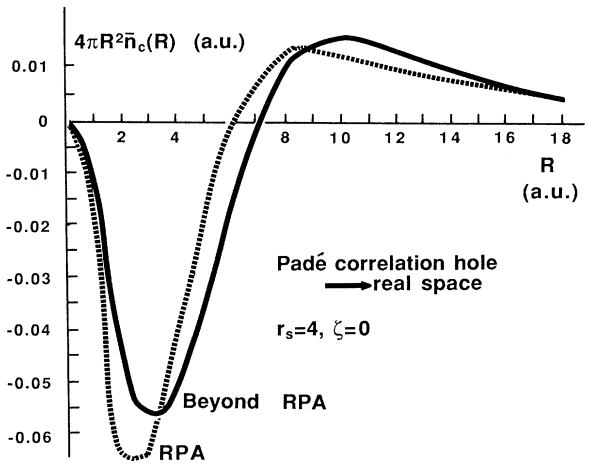


FIG. 3. The correlation hole density $\bar{n}_c(R)$ in real space, obtained by inverse Fourier transformation of the Padé representations (71) within (dashed curve) and beyond (solid curve) RPA.

Padé representation for the Fourier transform of the Coulomb hole density.

## ACKNOWLEDGMENTS

This work was supported by the National Science Foundation under Grant No. DMR 88-17866. We thank J. G. Zabolitzky for permission to reproduce parts of Figs. 14 and 15 of Ref. 12.

## APPENDIX: LOW-DENSITY LIMIT OF RPA CORRELATION ENERGY

To derive the $r_s^{-3/4}$ behavior of Eq. (70), consider the spin-unpolarized RPA correlation energy of Eqs. (10) and (61):

$$\varepsilon_c^{\mathrm{RPA}}(r_s,0)=-\frac{12}{\pi}\frac{1}{c^2 r_s^2}\int_0^\infty dQ\int_0^\infty dW\,Q^2\left[\frac{cr_s}{2\pi}\beta(Q,W)-\ln\left[1+\frac{cr_s}{2\pi}\beta(Q,W)\right]\right]. \tag{A1}$$

For $r_s\gg 1$ we might expect[20] (A1) to be dominated by its first term, leading to the result $\varepsilon_c^{\mathrm{RPA}}(r_s,0)\sim r_s^{-1}$ as $r_s\to\infty$. However, the condition $(r_s/2\pi)\beta(Q,W)\gg 1$ cannot be obeyed everywhere, no matter how large $r_s$ is.

According to Eq. (52), we have for large $Q$

$$\frac{cr_s}{2\pi}\beta(Q,W)=\frac{cr_s}{3\pi}\frac{Q^{-4}}{1+v^2}+O(r_s Q^{-5}). \tag{A2}$$

Clearly $(cr_s/2\pi)\beta(Q,W)<1$ for $Q>Q_0$, where

$$Q_0=\left[\frac{c}{3\pi}\right]^{1/4}(1+v^2)^{-1/4}r_s^{1/4}. \tag{A3}$$

Now we calculate the contribution from this region $Q>Q_0$ to the correlation energy of Eq. (A1):

$$\Delta\varepsilon_c^{\mathrm{RPA}}(r_s,0)=\frac{-12}{\pi}\frac{1}{c^2 r_s^2}\int_0^\infty dv\int_{Q_0}^\infty dQ\,Q^4\sum_{n=2}^\infty\frac{(-1)^n}{n}\left[\frac{cr_s}{2\pi}\beta(Q,W)\right]^n, \tag{A4}$$

where we have used the fact that $(cr_s/2\pi)\beta(Q,W)<1$ to make the Taylor expansion. It is straightforward to evaluate

$$\int_{Q_0}^\infty dQ\,Q^4\left[\frac{cr_s}{2\pi}\beta(Q,W)\right]^n=\int_{Q_0}^\infty dQ\,Q^4\left[\frac{cr_s}{3\pi}\frac{Q^{-4}}{1+v^2}\right]^n=\frac{1}{4n-5}\left[\frac{c}{3\pi}\right]^{5/4}(1+v^2)^{-5/4}r_s^{5/4}. \tag{A5}$$

Substitute (A5) into (A4) and find

$$\Delta\varepsilon_c^{\mathrm{RPA}}(r_s,0)=\frac{-\Delta C^{\mathrm{RPA}}}{r_s^{3/4}}, \tag{A6}$$

where

$$\Delta C^{\mathrm{RPA}}=\frac{12}{\pi}(3\pi)^{-5/4}c^{-3/4}\sum_{n=1}^\infty\frac{(-1)^{n+1}}{(n+1)(4n-1)}\int_0^\infty dv(1+v^2)^{-5/4}=0.06. \tag{A7}$$

Equations (A6) and (A7) include only the contribution to Eq. (70) from $Q<Q_0$, but the contribution from $Q>Q_0$ must have the same sign [since the integrand of Eq. (A1) is everywhere positive.] The derivation is readily extended to the spin-polarized case.

*Present address: Department of Chemistry, University of North Carolina, Chapel Hill, NC 27599.

[1]O. Gunnarsson and B. I. Lundqvist, Phys. Rev. B **13**, 4274 (1976).
[2]D. C. Langreth and J. P. Perdew, Solid State Commun. **17**, 1425 (1975).
[3]O. Gunnarsson, M. Jonson, and B. I. Lundqvist, Phys. Rev. B **20**, 3136 (1979).
[4]J. P. Perdew, Physica **172**, 1 (1991).
[5]J. P. Perdew, in *Proceedings of the 21st Annual International Symposium "Electronic Structure of Solids"* (Nova Science, Commack, NY, in press).
[6]J. P. Perdew and Y. Wang (unpublished).
[7]M. K. Harbola and V. Sahni, Phys. Rev. Lett. **62**, 489 (1989).
[8]U. von Barth and L. Hedin, J. Phys. C **5**, 1629 (1972).
[9]D. M. Ceperley and B. J. Alder, Phys. Rev. Lett. **45**, 566 (1980).
[10]K. S. Singwi and M. P. Tosi, Solid State Phys. **36**, 177 (1981). See Fig. 1.
[11]P. Nozières and D. Pines, Phys. Rev. **111**, 442 (1958).
[12]K. Emrich and J. G. Zabolitzky, Phys. Rev. B **30**, 2049 (1984). See Figs. 14 and 15.

[13]V. Contini, G. Mazzone, and F. Sacchetti, Phys. Rev. B **33**, 712 (1986).
[14]E. Chacón and P. Tarazona, Phys. Rev. B **37**, 4013 (1988).
[15]M. Gell-Mann and K. Brueckner, Phys. Rev. **106**, 364 (1957).
[16]D. Pines and P. Nozières, *The Theory of Quantum Liquids* (Benjamin, New York, 1966).
[17]D. C. Langreth and J. P. Perdew, Phys. Rev. B **15**, 2884 (1977).
[18]Y. Wang and J. P. Perdew, Phys. Rev. B **43**, 8911 (1991).
[19]A. K. Rajagopal, J. C. Kimball, and M. Banerjee, Phys. Rev. B **18**, 2339 (1978).
[20]S. Misawa, Phys. Rev. **140**, A1645 (1965).
[21]D. Ceperley, Phys. Rev. B **18**, 3126 (1978).
[22]S. H. Vosko, L. Wilk, and M. Nusair, Can. J. Phys. **58**, 1200 (1980).
[23]L. A. Cole and J. P. Perdew, Phys. Rev. A **25**, 1265 (1982).
[24]J. P. Perdew and A. Zunger, Phys. Rev. B **23**, 5048 (1981).
[25]M. Levy, Phys. Rev. A **43**, 4637 (1991).